

KEK Preprint 2018-4  
May 2018  
H

# Versatile $e^+e^-/\gamma\gamma/ep$ facilities at a Future Circular Collider

R. BELUSEVIC

*High Energy Accelerator Research Organization (KEK)*  
1-1 Oho, Tsukuba, Ibaraki 305-0801, Japan  
r.belusevic@gmail.com  
<https://www.rbelusevic-webpage.net>

# Contents

<b>1</b>	<b>Introduction</b>	<b>3</b>
<b>2</b>	<b>An SLC-type facility at FCC for creating <math>e^+e^-/\gamma\gamma/ep</math> collisions</b>	<b>5</b>
<b>3</b>	<b>An ILC-based <math>e^+e^-/\gamma\gamma/ep</math> facility at FCC</b>	<b>7</b>
<b>4</b>	<b>Main parameters of a linac-ring <math>ep</math> collider at FCC</b>	<b>7</b>
<b>5</b>	<b>Multi-MW proton beams for fixed-target experiments at FCC</b>	<b>13</b>
<b>6</b>	<b>Acknowledgements</b>	<b>13</b>

## References

**Abstract :** This note describes two versatile accelerator complexes that could be built at a Future Circular Collider (FCC) in order to produce  $e^+e^-$ ,  $\gamma\gamma$  and  $ep$  collisions. The first facility is an SLC-type machine comprising a superconducting L-band linear accelerator (linac) and two arcs of bending magnets inside the FCC tunnel. Accelerated by the linac, electron and positron beams would traverse the arcs in opposite directions and collide at centre-of-mass energies considerably exceeding those attainable at circular  $e^+e^-$  colliders. The proposed SLC-type facility would have the same luminosity as a conventional two-linac  $e^+e^-$  collider. The L-band linac may form a part of the injector chain for a 100-TeV proton collider inside the FCC tunnel (FCC-pp), and could deliver electron or positron beams for an  $ep$  collider (FCC-ep). The second facility is an ILC-based  $e^+e^-$  collider placed tangentially to the circular FCC tunnel. If the collider is positioned asymmetrically with respect to the FCC tunnel, electron (or positron) bunches could be accelerated by both linacs before they are brought into collision with the 50-TeV beams from the FCC-pp proton storage ring. The two linacs may also form a part of the injector chain for FCC-pp. Each facility could be converted into a  $\gamma\gamma$  collider or a source of multi-MW beams for fixed-target experiments.

## 1 Introduction

The maximum luminosity at a circular  $e^+e^-$  collider, such as the proposed FCC-ee facility [1], is severely constrained by beamstrahlung effects at high energies; also, it is very difficult to achieve a high degree of beam polarization [2]. At the  $e^+e^-$  facilities described in this paper, luminosity grows almost linearly with the beam energy [3] and the initial electron beam polarization can reach about 80% [4]. The availability of polarized beams is essential for some important precision measurements in  $e^+e^-$  and  $\gamma\gamma$  collisions [5].

The rich set of final states in  $e^+e^-$  and  $\gamma\gamma$  collisions would play an essential role in measuring the mass, spin, parity, two-photon width and trilinear self-coupling of the *Standard Model* (SM) Higgs boson, as well as its couplings to fermions and gauge bosons. Some of those measurements require centre-of-mass (c.m.) energies  $\sqrt{s_{ee}}$  considerably exceeding those attainable at circular  $e^+e^-$  colliders. For instance, one has to measure separately the HWW, HHH and Htt couplings at  $\sqrt{s_{ee}} \gtrsim 500$  GeV in order to determine the corresponding SM loop contributions to the effective HZZ coupling [6]. This would not be possible to accomplish using the proposed FCC-ee facility.

The Htt coupling cannot be *directly measured* in  $e^+e^-$  interactions below  $\sqrt{s_{ee}} \approx 500$  GeV, since the cross-section for the relevant process is negligible (see Fig. 1). Concerning the HHH coupling, this quantity can be *directly measured* at energies above the kinematic threshold for the reaction  $e^+e^- \rightarrow ZHH$ , or by using the WW-fusion channel at  $\sqrt{s_{ee}} \gtrsim 1$  TeV. *Indirect* and *model dependent* measurements of the HHH coupling are possible at lower energies by exploiting the loop corrections to single Higgs channels. However, the sensitivity of such measurements is very low, as can be inferred from Fig. 4 in [7].

Since the Higgs-boson mass affects the values of electroweak observables through radiative corrections, high-precision electroweak measurements provide a natural complement to direct studies of the Higgs sector. All the measurements made at LEP and SLC could be repeated at the facilities described in this note, but at much higher luminosities and using 80% polarized electron beams [8]. The importance of beam polarization for some high-precision measurements was already stressed.

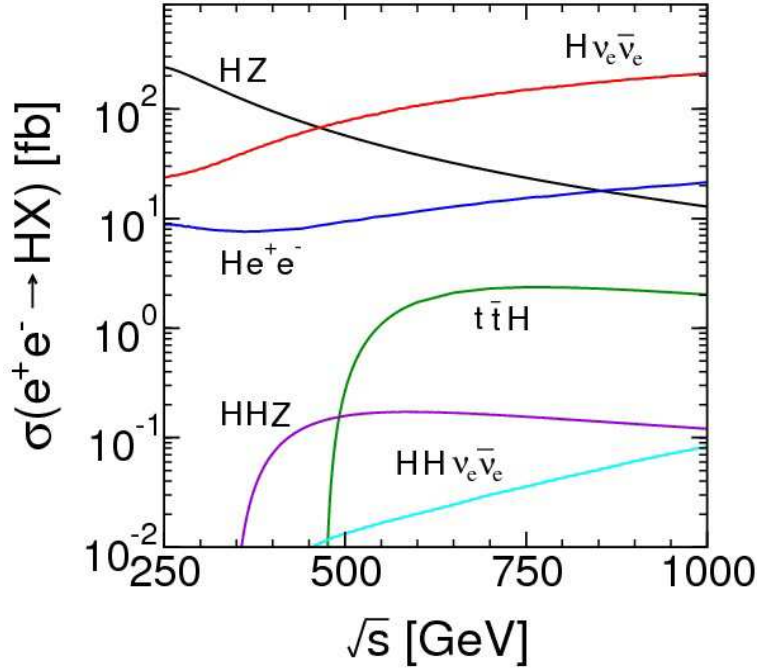


Figure 1: Centre-of-mass energy dependence of various cross-sections for single and double SM Higgs-boson production in  $e^+e^-$  annihilations [11].

If electron or positron bunches are brought into collision with the 50-TeV proton beams from the FCC-pp storage ring, one would obtain an important source of deep-inelastic  $ep$  interactions.<sup>1</sup> Such interactions would yield valuable information on the quark-gluon content of the proton, which is crucial for precision measurements at the FCC-pp. The physics potential of a TeV-scale  $ep$  collider is comprehensively discussed in [10].

An SLC-type facility or a conventional two-linac collider could be constructed in several stages, each with distinct physics objectives that require particular centre-of-mass energies (see Fig. 1):

- $e^+e^- \rightarrow Z, WW; \quad \gamma\gamma \rightarrow H$   $\sqrt{s_{ee}} \sim 90$  to  $180$  GeV
- $e^+e^- \rightarrow HZ$   $\sqrt{s_{ee}} \sim 250$  GeV
- $e^+e^- \rightarrow t\bar{t}; \quad \gamma\gamma \rightarrow HH$   $\sqrt{s_{ee}} \sim 350$  GeV
- $e^+e^- \rightarrow HHZ, Ht\bar{t}, H\nu\bar{\nu}$   $\sqrt{s_{ee}} \gtrsim 500$  GeV

For some processes within and beyond the SM, the required c.m. energy is considerably lower in  $\gamma\gamma$  collisions than in  $e^+e^-$  or proton-proton interactions. For example, the heavy neutral MSSM Higgs bosons can be created in  $e^+e^-$  annihilations only by associated production ( $e^+e^- \rightarrow H^0 A^0$ ), whereas in  $\gamma\gamma$  collisions they are produced as single resonances ( $\gamma\gamma \rightarrow H^0, A^0$ ) with masses up to 80% of the initial  $e^-e^-$  collider energy.

It is straightforward to convert an SLC-type facility or a conventional two-linac collider into a high-luminosity  $\gamma\gamma$  collider with highly polarized beams. The CP properties of any neutral Higgs boson produced at a photon collider can be directly determined by controlling the polarizations of Compton-scattered photons (see [12] and references therein).

<sup>1</sup>The proposed FCC-eh electron-proton collider [9] would provide a higher luminosity than the facilities described in this paper, but would have a considerably lower electron beam energy (around 60 GeV).

## 2 An SLC-type facility at FCC for creating $e^+e^-/\gamma\gamma/ep$ collisions

A schematic layout of an SLC-type  $e^+e^-/\gamma\gamma$  facility at a Future Circular Collider (FCC) is shown in Fig. 2. Damped and bunch-compressed electron and positron beams, accelerated by a single superconducting L-band linac, traverse two arcs of bending magnets in opposite directions and collide at an interaction point surrounded by a detector. The beams are then disposed of, and this machine cycle is repeated at a rate of up to 10 Hz. In contrast to a conventional two-linac collider, an SLC-type machine would have a single bunch compression system.

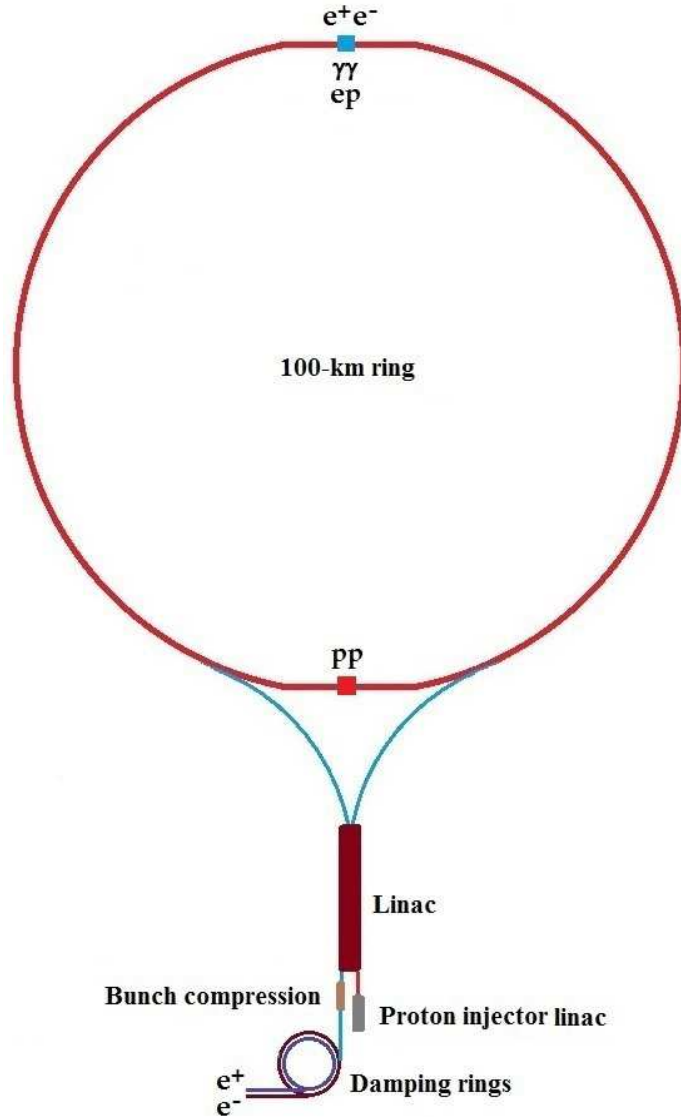


Figure 2: Schematic layout of an SLC-type facility at FCC [12]. The superconducting L-band linac could be a part of the FCC-pp injector chain (how to adjust the proton bunch length throughout the accelerator complex is discussed in Section 4). The entire facility would serve as a source of  $e^+e^-$ ,  $\gamma\gamma$ ,  $pp$  and  $ep$  interactions.

The linac in Fig. 2 would contain ILC-type superconducting L-band cavities placed within cryogenic vessels and fed by multi-beam klystrons. The current design for the *International Linear Collider* (ILC), based on the technology originally developed at DESY, uses L-band (1.3 GHz) superconducting niobium rf cavities that have average accelerating gradients of 31.5 MeV/m (see [13] and references therein). Nine cavities, each 1 m long, are mounted together in a string and

assembled into a common low-temperature cryostat or *cryomodule*. Liquid helium is used to cool cavities to  $-271^\circ\text{C}$ .

An ILC-type main linac is composed of rf units, each of which is formed by three contiguous cryomodules containing 26 nine-cell cavities. Every unit has an rf source, which includes a pulse modulator, a 10 MW multi-beam klystron, and a waveguide system that distributes the power to the cavities. An ILC-type design has the following characteristics:

- Transverse wakefield effects are drastically reduced due to the large size of L-band cavities, which means that cavity alignment tolerances can be relaxed. This is particularly relevant for an SLC-type facility, where both  $e^+$  and  $e^-$  bunches are alternately accelerated;
- Superconducting ILC-type rf cavities can be loaded using a long rf pulse ( $\sim 1.5$  ms) from a source with low peak rf power;
- Wall-plug to beam power transfer efficiency is about twice that of X-band cavities, for example, which makes an ILC-type linac much cheaper to operate;
- The long rf pulse allows a long ‘bunch train’ ( $\sim 1$  ms), with many bunches ( $\sim 3000$ ) and a relatively large bunch spacing ( $\sim 300$  ns). A trajectory correction (feedback) system within the train can therefore be used to bring the beams into collision.

At an SLC-type facility,  $e^+$  and  $e^-$  bunches are alternately accelerated inside the linac. In order to focus  $e^-$  and  $e^+$  beams in the two transverse planes, quadrupole magnets with alternating polarities have to be placed along the linac. The  $x$ -plane for electrons is then like the  $y$ -plane for positrons, and vice versa. At the *Stanford Linear Collider* (SLC), emittance growth in the linac was reduced using the beam diagnostics obtained by steering both beams together [14].

The spacing between electron bunches in a superconducting L-band accelerator can be made to match that between proton bunches in the FCC-pp storage ring. Also, the length of an electron ‘bunch train’ corresponds roughly to the FCC ring circumference. An ILC-type linac is thus a suitable source of electron beams for a high-luminosity  $ep$  collider. This is not the case with an X-band linac, where the electron bunch spacing ( $\sim 1$  ns) is much shorter than that between proton bunches at the FCC-pp (see Table 2).

The total energy loss due to *synchrotron radiation* in each arc of the proposed SLC-type facility is  $\Delta E = 14.4$  GeV for  $E_0 = 250$  GeV and  $\rho = 12$  km, where  $E_0$  is the initial electron (or positron) beam energy and  $\rho$  the *effective bending radius*. Synchrotron radiation is also responsible for *energy spread*,  $\sigma_E/E$ , in an electron beam. A plot of  $\sigma_E/E$  as a function of beam energy for  $\rho = 12$  is shown in Fig. 6 of [12]. For electron beams with  $E \lesssim 450$  GeV traversing the bending arcs of the proposed SLC-type facility, the increase in the *horizontal beam emittance* would not exceed  $2\ \mu\text{m}$ , the value of this parameter at the KEK-ATF damping ring (see Fig. 7 in [12]). Figures 6 and 7 in [12] were produced using a lattice of combined-function FODO cells as an input to K. Oide’s SAD tracking code.

The *geometric luminosity* at a conventional two-linac collider is given by

$$\mathcal{L}_{ee} \propto \frac{\gamma N_e^2 N_b f_{\text{rep}}}{\sqrt{(\varepsilon_x^n \beta_x^*)(\varepsilon_y^n \beta_y^*)}} \equiv \frac{\mathcal{P}_b}{\sqrt{s_{ee}}} \frac{\gamma N_e}{\sqrt{(\varepsilon_x^n \beta_x^*)(\varepsilon_y^n \beta_y^*)}} \quad (1)$$

where  $\beta_x^*$  and  $\beta_y^*$  are the horizontal and vertical *beta functions* at the interaction point (IP), respectively,  $\varepsilon_x^n$  and  $\varepsilon_y^n$  are the normalized transverse *beam emittances*,  $N_e$  is the number of electrons in a ‘bunch’,  $N_b$  is the number of bunches per rf pulse,  $f_{\text{rep}}$  is the pulse *repetition rate*,  $\sqrt{s_{ee}}$  is the c.m. energy,  $\mathcal{P}_b = N_e N_b f_{\text{rep}} \sqrt{s_{ee}}$  is the *beam power*, and  $\gamma \equiv E/m_e c^2$  is the *Lorentz factor* of the electron beam with energy  $E$ .

There are  $N_b/2$  electron or positron bunches in each arc of an SLC-type facility. If its repetition rate is twice that of a conventional two-linac collider, so that the same wall-plug power is used, the two machines would have the same luminosity (see Eq. (1)).

An important feature of the proposed facilities is the possibility of using backscattered laser beams to produce high-energy  $\gamma\gamma$  collisions [15]. In order to attain maximum luminosity at a  $\gamma\gamma$  collider, every electron bunch in the accelerator should collide with a laser pulse of sufficient intensity for 63% of the electrons to undergo a Compton scattering. This requires a laser system with high average power, capable of producing pulses that would match the temporal spacing of electron bunches. These requirements could be satisfied by an optical *free electron laser* [16]. The luminosity of a gamma-gamma collider is  $\mathcal{L}_{\gamma\gamma} = (N_\gamma/N_e)^2 \mathcal{L}_{ee} \approx (0.63)^2 \mathcal{L}_{ee}$ , where  $N_\gamma$  is the number of backscattered laser photons.

### 3 An ILC-based $e^+e^-/\gamma\gamma/ep$ facility at FCC

The ILC-based facility at a Future Circular Collider (FCC) shown in Fig. 3 features a superconducting two-linac  $e^+e^-$  collider placed tangentially to the FCC tunnel [17]. Using an optical free-electron laser, the linacs could be converted into a high-luminosity  $\gamma\gamma$  collider.

As mentioned in the Introduction, the maximum luminosity at a circular  $e^+e^-$  collider is severely constrained by beamstrahlung effects at high energies; also, it is very difficult to achieve a high degree of beam polarization. At the  $e^+e^-$  facilities described in this paper, luminosity grows almost linearly with the beam energy and the electron beam polarization can reach 80%.

The maximum c.m. energy of an SLC-type facility is limited by the radius of the bending arcs, which is not the case with a conventional two-linac  $e^+e^-$  collider. Note also that the asymmetric accelerator configuration in Fig. 3 allows one to double the energy of electron or positron beams before their extraction (see Section 4).

The baseline parameters for the proposed ILC collider, shown in Table 1, reflect the need to balance the constraints imposed by the various accelerator sub-systems, as explained in [18]. The rf power is provided by 10 MW multi-beam klystrons, each driven by a 120 kV pulse modulator. The estimated AC power is 122 MW at  $\sqrt{s_{ee}} = 250$  GeV and 163 MW at  $\sqrt{s_{ee}} = 500$  GeV.

In order to maximize luminosity at low centre-of-mass energies, the beam power could be increased by increasing the pulse repetition rate  $f_{\text{rep}}$  while reducing the accelerating gradient of the main linacs. At  $\sqrt{s_{ee}} = 250$  GeV, the power consumption of the main 250-GeV linacs is reduced by over a factor of two when they are running at half their nominal gradient. Under these conditions, one can run the accelerator at the maximum repetition rate of 10 Hz (determined by the cryogenic system and the beam damping time  $t_{\text{damp}} \approx 80$  ms), thus doubling its luminosity.

The two superconducting L-band linacs in Fig. 3 may also form a part of the FCC-pp injector chain. Since the collider is positioned asymmetrically with respect to the FCC tunnel, electron (or positron) bunches could be accelerated by both linacs before they are brought into collision with the 50-TeV beams from the FCC-pp proton storage ring, as mentioned above. The entire accelerator complex would serve as a source of  $e^+e^-$ ,  $\gamma\gamma$ ,  $pp$  and  $ep$  interactions.

### 4 Main parameters of a linac-ring $ep$ collider at FCC

The idea to combine a 140-GeV electron linac and a 20-TeV proton storage ring in order to produce  $ep$  interactions at very high c.m. energies was put forward in 1979 as a possible option at the SSC proton collider [19]. In 1987 it was proposed to place a 2-TeV linear  $e^+e^-$  collider (VLEPP) tangentially to a 6-TeV proton-proton collider (UNK) at IHEP in Protvino [20], with the aim of obtaining both  $ep$  and  $\gamma p$  collisions. Similar proposals for lepton-hadron and photon-hadron colliders at HERA, LHC and FCC have since been made (see [21] and references therein).

The SLC-type facility in Fig. 2 could be used to produce TeV-scale  $ep$  interactions. Accelerated by the superconducting L-band linac, electron or positron beams would traverse one of the two

Table 1: Baseline ILC parameters [18]

Centre-of-mass energy	$\sqrt{s_{ee}}$	GeV	250	500
Pulse repetition rate	$f_{\text{rep}}$	Hz	5	5
Bunch population	$N_e$	$\times 10^{10}$	2	2
Number of bunches	$N_{b,e}$		1312	1312
Bunch interval	$\Delta t_{b,e}$	ns	554	554
RMS bunch length	$\sigma_{z,e}$	mm	0.3	0.3
Norm. horizontal emittance at IP	$\varepsilon_x^n$	$\mu\text{m}$	10	10
Norm. vertical emittance at IP	$\varepsilon_y^n$	nm	35	35
Horizontal beta function at IP	$\beta_x^*$	mm	13	11
Vertical beta function at IP	$\beta_y^*$	mm	0.41	0.48
RMS horizontal beam size at IP	$\sigma_x^*$	nm	729	474
RMS vertical beam size at IP	$\sigma_y^*$	nm	7.7	5.9
Vertical disruption parameter	$D_e$		24.5	24.6
Luminosity	$\mathcal{L}_{ee}$	$\times 10^{34} \text{ cm}^{-2} \text{ s}^{-1}$	0.75	1.8

arcs of bending magnets inside the FCC tunnel and collide with the FCC-pp proton beams.

The facility shown in Fig. 3 is an ILC-based version of the original VLEPP $\otimes$ UNK design. Since the collider is positioned asymmetrically with respect to the FCC tunnel, electron (or positron) bunches could be accelerated by both linacs (which contain *standing wave cavities*) before they are brought into collision with the 50-TeV beams from the FCC-pp proton storage ring.

In Section 2 it was noted that an ILC-type linac is a suitable source of electron beams for an electron-proton collider, because: (1) the spacing between electron bunches can be made to match that between the proton bunches in the FCC-pp storage ring, and (2) the length of an electron ‘bunch train’ corresponds roughly to the FCC ring circumference.

In *head-on collisions* of ultra-relativistic electrons and protons, the centre-of-mass energy is  $\sqrt{s_{ep}} = 2\sqrt{E_e E_p}$ . The total electron beam current  $I_e = \mathcal{P}_e/E_e$  is limited by the maximum allowed beam power  $\mathcal{P}_e$  for a given electron beam energy  $E_e$ . Assuming that round electron and proton beams of equal transverse sizes are colliding head-on at the interaction point (IP),<sup>2</sup> the luminosity of the collider is given by [22][23]

$$\mathcal{L}_{ep} = f_c \frac{N_e N_p}{4\pi\sigma_p^2} \mathcal{H} \equiv \frac{I_e}{4\pi e} \frac{N_p}{\varepsilon_p^n} \frac{\gamma_p}{\beta_p^*} \mathcal{H} \quad (2)$$

In these expressions,  $N_e$  and  $N_p$  are the electron and proton bunch populations, respectively;  $f_c$  is the bunch collision frequency;  $\mathcal{H}$  is a correction factor discussed below; and  $\sigma_p = \sqrt{\varepsilon_p^n \beta_p^* / \gamma_p}$  is the proton beam size at IP, expressed in terms of the normalized proton beam emittance,  $\varepsilon_p^n$ , the proton beta function at IP,  $\beta_p^*$ , and the Lorentz factor of the proton beam,  $\gamma_p$ . Note that the luminosity is proportional to the electron beam power  $\mathcal{P}_e = eN_e f_c E_e = I_e E_e$  (e is the electron charge), the proton beam energy ( $\gamma_p$ ), and the proton beam brightness  $N_p/\varepsilon_p^n$ .

In Eq. (2),  $\mathcal{H}$  is a product of three correction factors with values typically close to unity:

$$\mathcal{H} \equiv H_{\text{hourglass}} \cdot H_{\text{pinch}} \cdot H_{\text{filling}} \quad (3)$$

<sup>2</sup>The two beams are chosen to have roughly equal transverse sizes in order to reduce adverse effects a much smaller electron beam could have on the proton beam lifetime. Electron bunches are discarded after each collision.



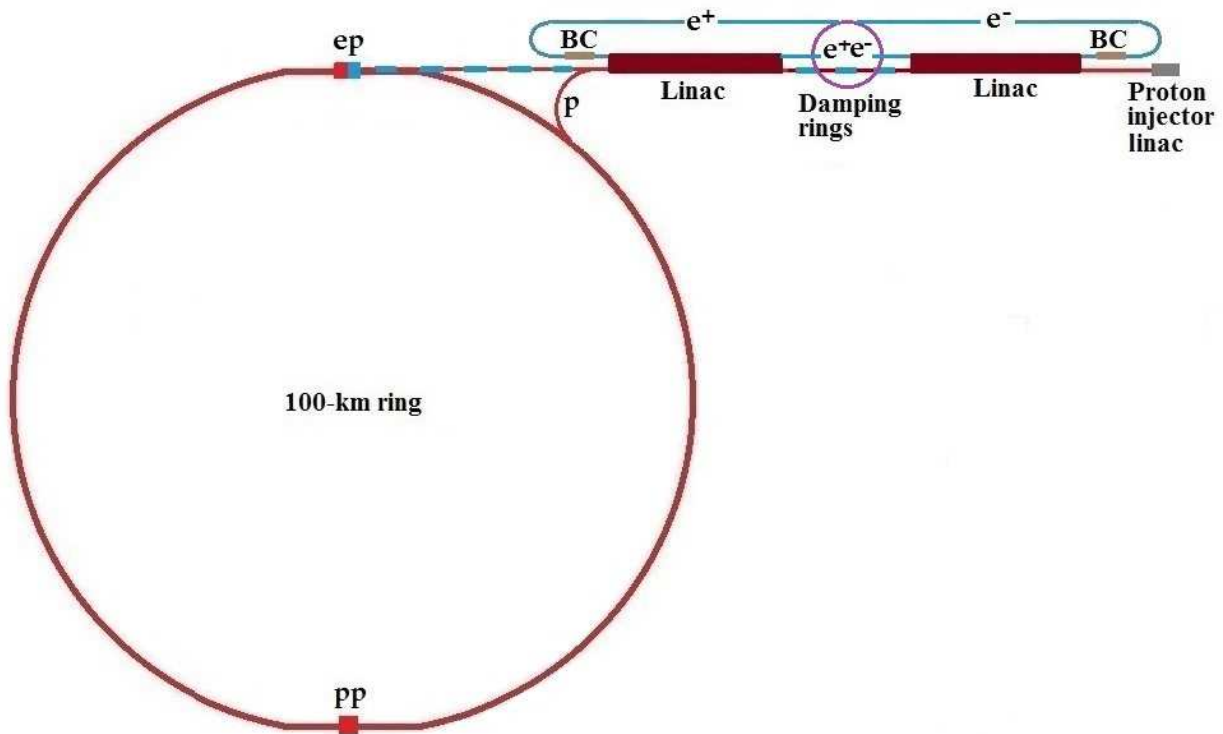


Figure 3: An ILC-based facility at FCC (BC stands for *bunch compression*). Electron (or positron) bunches are accelerated by both linacs before their collision with the 50-TeV proton beam from the FCC-pp storage ring. The two superconducting L-band linacs may form the low-energy part of the FCC-pp injector chain [17]. The issue of proton bunch length is discussed in Section 4.

The factor  $H_{\text{filling}}$  takes into account the filling patterns of the electron and proton beams. If the number of proton bunches  $N_{b,p} = 10600$  and the bunch interval  $\Delta t_{b,p} = 25$  ns (see Table 2), the ‘length’ of the proton beam is  $2.65 \times 10^5$  ns. This corresponds to 80 km, which means that only 80% of the FCC circumference is filled with proton bunches ( $H_{\text{filling}} = 0.8$ ). In this particular case 20% of the electron bunches would not collide with the proton beam.

The factor  $H_{\text{hourglass}}$  accounts for a loss of luminosity when the bunch length is comparable to or larger than  $\beta^*$ . The beta function  $\beta(s) = \beta^* + s^2/\beta^*$  grows parabolically as a function of distance  $s$  from the interaction point, which causes the beam size to increase:

$$\sigma(s) = \sqrt{\beta(s) \cdot \varepsilon} \approx s \sqrt{\varepsilon/\beta^*} \quad (4)$$

As the beam size increases, the contribution to the luminosity from regions with large  $\sigma$  decreases (*hourglass effect*). For zero crossing angle and  $\sigma_{z,p} \gg \sigma_{z,e}$ ,

$$H_{\text{hourglass}}(x) = \sqrt{\pi} x e^{x^2} \text{erfc}(x) \quad (5)$$

with

$$x \equiv \frac{2\beta_e^*}{\sigma_{z,p}} \frac{\varepsilon_e/\varepsilon_p}{\sqrt{1 + (\varepsilon_e/\varepsilon_p)^2}}, \quad \text{erfc}(x) = \frac{2}{\sqrt{\pi}} \int_x^\infty e^{-t^2} dt \quad (6)$$

where  $\varepsilon_e$  and  $\varepsilon_p$  denote *geometric emittances* [10][26] (the normalized emittance  $\varepsilon^n = \gamma\varepsilon$  is invariant under acceleration);  $\text{erfc}(z)$  is the ‘complementary error function’ (defined as the area under the ‘tails’ of a Gaussian distribution).

The enhancement factor  $H_{\text{pinch}}$  in Eq. (3) is due to the attractive *beam-beam force*. Since the electron bunch charge is relatively small and the proton energy is high, the beam-beam force acting

Table 2: Baseline FCC-pp parameters [24][25]. Numbers inside round brackets represent parameters for 5 ns bunch spacing.

Beam energy	$E_p$	TeV	50
Initial bunch population	$N_p$	$\times 10^{10}$	10 (2)
Number of bunches	$N_{b,p}$		10600 (53000)
Bunch interval	$\Delta t_{b,p}$	ns	25 (5)
RMS bunch length	$\sigma_{z,p}$	mm	80
Norm. transverse emittance	$\varepsilon_p^n$	$\mu\text{m}$	2.2 (0.44)
Beta function at IP	$\beta_p^*$	m	0.3
Beam size at IP	$\sigma_p$	$\mu\text{m}$	6.8 (3)
Beam-beam tune shift/IP	$\Delta Q_p$		0.005
Luminosity/IP	$\mathcal{L}_{ep}$	$\times 10^{32} \text{ cm}^{-2} \text{ s}^{-1}$	2.3

on electrons has a much greater strength than that acting on protons. Consequently, the electron bunch is focused by the protons during a collision,. This leads to a reduction in the transverse electron beam size (‘pinch effect’) and hence to an increase in the luminosity. The effect can be simulated using the program *Guinea-Pig* (see [9] and references therein, as well as Table 3 below).

One can ignore the longitudinal structure of electron bunches because they are much shorter than proton bunches. In this case the *transverse disruption* of the electron beam during a collision is described by the parameter [27][28]

$$D_e = \frac{r_e}{\gamma_e} \frac{N_p \sigma_{z,p}}{\sigma_p^2} \quad (7)$$

where  $\gamma_e$  is the Lorentz factor of the electron beam,  $r_e \approx 2.82 \times 10^{-15}$  m is the classical radius of the electron, and  $\sigma_{z,p}$  is the proton bunch length. For  $\beta_p^* = 10$  cm, the disruption parameter can be as large as  $D_e \approx 20$  in an *ep* linac-ring collider [23].

As already mentioned, the luminosity of an *ep* collider is proportional to the proton *beam brightness*  $N_p/\varepsilon_p^n$  (see Eq. (2)). Together with a given bunch length and energy spread, the beam brightness is a measure of the phase-space density. In the low-energy part of a proton injector, the quantity  $N_p/\varepsilon_p^n$  is limited by space-charge forces that induce a *transverse tune shift*<sup>3</sup>

$$\Delta Q_{sc} \propto \frac{N_p}{\varepsilon_p^n} \frac{1}{(v_p/c)^2 \gamma_p^2} \quad (8)$$

Here  $v_p$  is the proton velocity and  $c$  is the speed of light in vacuo [29][30]. In order to reduce the effect of space-charge forces at low energies and deliver proton bunches a few mm long, the facility in Fig. 3 features a single 3-GeV proton injector linac similar to that currently being built at the *European Spallation Source* (ESS) [31].

At high energies, the beam brightness in a storage ring slowly diminishes due to Coulomb scattering of protons within a bunch (*intra-beam scattering*) [32]. In the presence of *dispersion* (see footnote 4), the intra-beam scattering also leads to an increase in emittance. This sets the

<sup>3</sup>The ‘tune’ or  $Q$  value is defined as the number of betatron oscillations per revolution in a circular accelerator. The charge and current of a high-intensity beam in an accelerator create self-fields and image fields that alter the beam dynamics and influence the single-particle motion as well as coherent oscillations of the beam as a whole. The effect of space-charge forces is to change  $Q$  by an amount  $\Delta Q_{sc}$  (‘tune shift’) [29].

ultimate limit on the phase-space density in a proton storage ring. The growth of a beam of charged particles due to intra-beam scattering is characterized by the horizontal *growth rate* [33]

$$\tau_x^{-1} \propto \frac{N_p}{\varepsilon_x^n \varepsilon_y^n \varepsilon_l^n} \quad (9)$$

where  $\varepsilon_{x,y}^n$  are the normalized beam emittances,  $\varepsilon_l^n \equiv \beta \gamma \sigma_{z,p} \sigma_{\Delta p/p}$  and  $\sigma_{\Delta p/p}$  is the r.m.s. relative momentum  $\Delta p/p$ . Note that the growth rate depends linearly on the normalized phase-space density. In the FCC-pp storage ring synchrotron radiation damping is expected to be much stronger than the intra-beam scattering, making the latter effect less of an issue [24].

The space-charge forces that limit the beam brightness are determined by the longitudinal charge density and thus by the proton bunch length  $\sigma_{z,p}$ . To attain maximum brightness,  $\sigma_{z,p}$  should be as large as possible. On the other hand, there is a loss of luminosity when the bunch length is comparable to or larger than  $\beta^*$  (this *hourglass effect* was described earlier). Furthermore, the transverse disruption of the electron beam during an *ep* collision is proportional to  $\sigma_{z,p}$ , as shown in Eq. 7. While optimizing the bunch length within these constraints, the beam stability must be preserved (see below).

A particle in one colliding beam experiences a force due to the electromagnetic interactions with all the particles in the opposing beam. This force depends upon the displacement of the particle from the equilibrium orbit of the opposing bunch. For small particle displacements, the beam-beam interaction is nearly linear, and its strength is characterized by a parameter known as the *beam-beam tune shift* [34]:

$$\Delta Q_p \equiv \frac{r_p N_e \beta_p^*}{4\pi \sigma_e^2 \gamma_p} \approx \frac{r_p N_e}{4\pi \varepsilon_p^n} \quad (10)$$

where  $r_p \approx 1.53 \times 10^{-18}$  m is the classical radius of the proton and  $\sigma_p \approx \sigma_e$  was used. Since electron bunches are discarded after each collision, only the tune shift of the proton beam,  $\Delta Q_p$ , is considered here. The tune shift is approximately given by

$$\Delta Q_p \approx 1.2 \times 10^{-3} \cdot \frac{N_e [10^{10}]}{\varepsilon_p^n [10^{-6} \text{ m}]} \quad (11)$$

The parameter  $\Delta Q_p$  must be limited to about  $4 \times 10^{-3}$  in order to stem the emittance growth due to random fluctuations of the electron bunch parameters [35]. This imposes an upper limit of  $N_e \lesssim 3 \times 10^{10}$  if one assumes  $\varepsilon_p^n \approx 10^{-6}$  m (see also Table 4 in [36]).

A small error  $\Delta k$  in the quadrupole gradient leads to a tune shift  $\Delta Q_k$ . To a beam particle with momentum  $p = p_0 + \Delta p$  it appears that all the quadrupoles in the ring have a quadrupole error proportional to  $\Delta p/p_0$  [37]. The dimensionless quantity  $\xi$  defined by  $\Delta Q_k \equiv \xi(\Delta p/p_0)$  is called the *chromaticity* of the beam optics. This quantity increases with the strength of the beam focusing. The main contribution to the chromaticity comes from the final focus quadrupoles, where the  $\beta$ -function is large [38]:

$$\xi \approx \beta_q k_q \ell_q \approx \frac{\ell^* + \ell_q/2}{\beta_y^*} \quad (12)$$

Here  $\beta_q$ ,  $k_q$  and  $\ell_q$  denote the beta function, field gradient and length of the final quadrupole, respectively;  $\ell^*$  is the focal length and  $\beta_y^*$  the value of the vertical  $\beta$ -function at the interaction point. Thus, the chromaticity increases as  $\beta_y^*$  decreases.

Since  $\xi$  grows linearly with the distance between the final-focus quadrupole and the interaction point, it is desirable to make this distance as small as possible. For the interaction region at an electron-proton collider, a novel design technique called the *achromatic telescopic squeezing* (ATS) has been proposed “in order to find the optimal solution that would produce the highest luminosity while controlling the chromaticity, minimizing the synchrotron radiation power and

Table 3: Parameters of the proposed linac-ring  $ep$  collider.

Electron beam parameters			
Beam energy	$E_e$	GeV	500
Initial bunch population	$N_e$	$\times 10^{10}$	2
Number of bunches	$N_{b,e}$		3200
Bunch interval	$\Delta t_{b,e}$	ns	211.376
RF frequency	$f_{\text{RF}}$	MHz	1301
Pulse repetition rate	$f_{\text{rep}}$	Hz	5
Duty cycle	$d$	%	0.34
Beam power	$\mathcal{P}_e$	MW	25.5
Proton beam parameters			
Beam energy	$E_p$	TeV	50
Initial bunch population	$N_p$	$\times 10^{10}$	10
Number of bunches	$N_{b,p}$		5300
RMS bunch length	$\sigma_{z,p}$	mm	80
Bunch interval	$\Delta t_{b,p}$	ns	49.7355
RF frequency	$f_{\text{RF}}$	MHz	401.968
Collider parameters			
Beta function at IP	$\beta_p^*$	m	0.1
Norm. transverse emittance	$\varepsilon_p^n$	$\mu\text{m}$	1
Beam-beam tune shift	$\Delta Q_p$		0.0024
Electron beam disruption	$D_e$		11.3
Hourglass factor	$H_{\text{hourglass}}$		0.81
Pinch factor	$H_{\text{pinch}}$		1.3
Proton filling	$H_{\text{filling}}$		0.79
Luminosity	$\mathcal{L}_{ep}$	$\times 10^{32} \text{ cm}^{-2} \text{ s}^{-1}$	1.08

maintaining the dynamic aperture required for [beam] stability” [39][40] (*dynamic aperture* is the stability region of phase space in a circular accelerator).

The issue of beam stability was addressed earlier concerning the optimization of the proton bunch length. The proton bunches inside the ILC-type linac shown in Figs 2 and 3 are much shorter than those inside the FCC storage ring (the 3-GeV injector linac mentioned earlier would deliver bunches a few millimetres long). Thus,  $\sigma_{z,p}$  has to be increased in order to attain the baseline FCC-pp value (see Table 2). In principle, the easiest way to increase the bunch length in a circular accelerator is to switch all RF systems off and let the bunches ‘decay’ due to *dispersion*.<sup>4</sup>

<sup>4</sup>A particle with a momentum difference  $\Delta p/p$  has a transverse position  $x(s) + D(s)\Delta p/p$ , where  $x(s)$  is the position a particle of nominal momentum would have and  $D(s)$  is the *dispersion function*.

A faster and more subtle method — which could be implemented using a 3-TeV proton booster placed inside the FCC tunnel — is described in [41].

The analytic expressions for beam-beam tune shift, electron beam disruption and beam growth rate given above do not accurately describe the *time-dependent beam dynamics* during collisions. To study the time-dependent effects caused by varying beam sizes, collision point simulations for linac-ring  $ep$  colliders have been performed using the ALOHEP software [42]. This numerical program optimizes a set of electron and proton beam parameters in order to maximize luminosity. Some of the results obtained by the program are presented in [43].

The luminosity  $\mathcal{L}_{ep}$  is independent of the electron bunch charge and the collision frequency as long as their product, expressed in terms of the beam power  $\mathcal{P}_e$ , is constant. One can therefore rewrite Eq. (2) as follows [22][44]

$$\mathcal{L}_{ep} = 4.8 \times 10^{30} \text{ cm}^{-2} \text{ s}^{-1} \cdot \frac{N_p}{10^{11}} \frac{10^{-6} \text{ m}}{\varepsilon_p^n} \frac{\gamma_p}{1066} \frac{10 \text{ cm}}{\beta_p^*} \frac{\mathcal{P}_e}{22.6 \text{ MW}} \frac{250 \text{ GeV}}{E_e} \cdot \mathcal{H} \quad (13)$$

The electron beam current  $I_e = eN_e f_{b,e} = 15 \text{ mA}$ , where  $f_{b,e}$  is the inverse of the bunch interval (see Table 3). The electron beam power  $\mathcal{P}_e = E_e I_e d = 25.5 \text{ MW}$ , where  $d$  is the linac duty cycle. The proton beam current  $I_p = 320 \text{ mA}$ , and the total energy stored per proton beam is 4.2 GJ. To calculate  $H_{\text{hourglass}}$ , we set  $\beta_e^* \approx \beta_p^*$  [40]. The value of  $H_{\text{pinch}}$  was taken from [9].

## 5 Multi-MW proton beams for fixed-target experiments at FCC

To search for new physics beyond the Standard Model usually requires the use of high-energy hadron or electron-positron colliders. However, many important discoveries in particle physics have been made using proton beams with relatively low energies but high intensities. With this in mind, it is envisaged that the facilities described in this note could also provide multi-MW proton beams for fixed-target experiments to study neutrino oscillations, rare kaon decays, the electric and magnetic dipole moments of the muon, etc.

The beam power in a circular accelerator is limited by space charge effects that produce beam instabilities. This limitation is intrinsic to the existing proton synchrotron complexes at CERN, Fermilab and J-PARC. To increase maximally the beam power of a ‘proton driver’, one could use the 3-GeV injector linac and the high-energy *pulsed* superconducting L-band structures shown in Figures 2 and 3. A similar facility was originally proposed at KEK by the present author [45].

For a pulsed linear accelerator, the following expression holds:

$$\mathcal{P}_b [\text{MW}] = E_b [\text{MV}] \times I [\text{A}] \times \tau_p [\text{s}] \times \mathcal{R} [\text{Hz}] \quad (14)$$

where  $\mathcal{P}_b$  is the *beam power*,  $E_b$  is the *beam energy*,  $I$  is the *average current per pulse*,  $\tau_p$  is the *beam pulse length*, and  $\mathcal{R}$  is the *pulse repetition rate*. Assuming  $E_b = 60 \times 10^3 \text{ MV}$ ,  $I = 25 \text{ mA}$ ,  $\tau_p = 1.2 \text{ ms}$  and  $\mathcal{R} = 10 \text{ s}^{-1}$ , expression (14) yields  $\mathcal{P}_b = 18 \text{ MW}$ . This is more than an order of magnitude higher than the beam power at any existing proton synchrotron complex. The physics potential of a multi-MW proton driver is discussed, for instance, in the references cited in [45].

## 6 Acknowledgements

I am grateful to K. Oide and D. Zhou for helping me estimate some relevant beam properties at the SLC-type facility described in this note, and would like to thank K. Yokoya for his valuable comments and suggestions.

## References

- [1] A. Blondel and F. Zimmermann, CERN-OPEN-2011-047; arXiv:1112.2518 (2012).
- [2] M. Koratzinos, arXiv:1511.01021v1 (2015).
- [3] M. Boscolo, J.-P. Delahaye and M. Palmer, arXiv:1808.01858 (2018).
- [4] B. Aurand et al., Proc. Intl. Linear Collider Workshop (LCWS08 and ILC08), Chicago, Illinois, 2008; arXiv:0903.2959 (2009).
- [5] G. Moortgat-Pick et al., Eur. Phys. J. C **75**: 371 (2015).
- [6] M. McCullough, arXiv:1312.3322v6 (2014).
- [7] S. Di Vita et al., DESY 17-131, FERMILAB-PUB-17-462-T and arXiv:1711.03978 (2017).
- [8] J. Erler et al., Phys. Lett. B **486**, 125 (2000).
- [9] O. Bruning et al., CERN-ACC-2017-0019 (2017).
- [10] J.L. Abelleira Fernandez, J. Phys. G: Nucl. Part. Phys. **39**, 075001 (2012).
- [11] D. Asner et al., arXiv:1310.0763v3 (2013).
- [12] R. Belusevic, J. Mod. Phys. **8**, pp 1–16 (2017).
- [13] B. Barish and J. Brau, Int. J. Mod. Phys. A **28**, 1330039 (2013).
- [14] F. Zimmermann, private communication.
- [15] I. Ginzburg et al., NIM **205**, 47 (1983); NIM **219**, 5 (1984).
- [16] E. Saldin, E. Schneidmiller and M. Yurkov, Nucl. Instrum. Meth. A **472**, 94 (2001).
- [17] R. Belusevic, J. High En. Phys. Grav. Cosm. **5**, 425–437 (2019).
- [18] C. Adolphsen et al., *The International Linear Collider Technical Design Report*, Volume 3.II; arXiv:1306.6328.
- [19] G. Weber et al., Proc. 2nd ICFA Workshop on Possibilities and Limitations of Accelerators and Detectors, Les Diablerets, Switzerland, 4–10 Oct. 1979, pp 199–221.
- [20] S.I. Alekhin et al., IHEP Preprint 87–48, Serpukhov (1987).
- [21] A.N. Akay, H. Karadeniz and S. Sultansoy, Int. J. Mod. Phys. A **25**, No. 4, pp 4589–4602 (2010).
- [22] M. Tigner, B. Wiik and F. Willeke, Proc. 1991 IEEE Part. Accel. Conf., San Francisco, California (1991).
- [23] F. Zimmermann et al., Proc. EPAC2008, Genoa, Italy, pp 2847–2849 (2008).
- [24] M. Benedikt, D. Schulte and F. Zimmermann, Phys. Rev. Spec. Topics — Accel. Beams **18**, 101002 (2015).
- [25] F. Zimmermann, Nucl. Instrum. Meth. B **355**, pp 4–10 (2015).

- [26] M. A. Furman, Proc. 1991 IEEE Particle Accelerator Conference, San Francisco, California, pp 422–424 (1991).
- [27] K. Yokoya and P. Chen, *Beam-beam phenomena in linear colliders*, Lectures at the US-CERN School on Particle Accelerators, Hilton Head Island, South Carolina, USA, 1990; printed in Lecture Notes in Physics 400, Springer-Verlag, pp 415–445 (1992).
- [28] Y. Hao and V. Ptitsyn, Phys. Rev. Spec. Topics — Accel. Beams **13**, 071003 (2010).
- [29] K. Schindl, *Space charge*, Proc. Joint US-CERN-Japan-Russia School on Particle Accelerators, Beam Measurements, Montreux, 1998, edited by S. Kurokawa, S.Y. Lee, E. Perevedentsev, S. Turner, World Scientific, pp 127–151 (1999).
- [30] M. Benedikt and R. Garoby, CERN-AB-2005-009.
- [31] H. Danared, M. Lindroos and C. Theroine, ESS: *neutron beams at the high-intensity frontier*, CERN Courier, June 2014, pp 21–24.
- [32] A. Piwinski, in *Proc. 9<sup>th</sup> Int. Conf. on High Energy Accelerators, Stanford* (1975).
- [33] G. Parzen, Nucl. Instr. Meth. **A 256**, pp 231–240 (1987).
- [34] F. Ruggiero and F. Zimmermann, Phys. Rev. Spec. Topics — Accel. Beams **5**, 061001 (2002).
- [35] R. Brinkmann, Turk. J. Phys. **22**, pp 661–666 (1998).
- [36] Ö. Yavas, Turk. J. Phys. **22**, pp 667–673 (1998).
- [37] K. Wille, *The Physics of Particle Accelerators*, Oxford Univ. Press, 2000.
- [38] F. Zimmermann, *Accelerator Physics and Technologis for Linear Colliders*, Physics 575 lecture notes, University of Chicago (2002).
- [39] S. Fartoukh, *Achromatic telescopic squeezing scheme and application to the LHC and its luminosity upgrade*, Phys. Rev. Spec. Topics — Accel. Beams **16**, 111002 (2013).
- [40] E. Cruz-Alaniz et al., Phys. Rev. Spec. Topics — Accel. Beams **18**, 111001 (2015).
- [41] H. Damerau, Ph.D. Thesis, Technical Univ. Darmstadt, 2005.
- [42] ALOHEP, <https://alohep.hepforge.org>; hosted by HepForge, IPPP Durham University.
- [43] Y. C. Acar et al., Nucl. Instr. Meth. **A 871**, pp 47–53 (2017).
- [44] The THERA Book, edited by U. Katz, M. Klein, A. Levy and S. Schlenstedt, DESY 01-123F, Vol. 4, DESY-LC-REV-2001-062 (2001).
- [45] R. Belusevic, J. Appl. Math. Phys. **5**, pp 1222–1242 (2017).